ARTICLES

Crystal Structure of an *n*-Paraffin Binary Eutectic Solid. An Electron Diffraction Determination

Douglas L. Dorset

Electron Diffraction Department, Hauptman-Woodward Medical Research Institute, Inc., 73 High Street, Buffalo, New York 14203-1196

Received: August 30, 1996; In Final Form: April 14, 1997[⊗]

The crystal structure of a paraffin binary eutectic formed from a nearly 1:1 combination of *n*-$C_{30}H_{62}$/*n*-$C_{40}H_{82}$ was determined with electron diffraction intensities from epitaxially oriented microareas. A pure *n*-$C_{40}H_{82}$ component could be isolated, and its diffraction pattern could be shown to match the structure expected for the pure even-chain paraffin in the $Pca2_1$ orthorhombic crystal structure. Although the microarea itself could not be isolated in electron diffraction experiments, the superlattice component of the lamellar row was separated from that of the pure longer chain species. After assigning a crystallographic phase envelope to these reflections to calculate the reverse Fourier transform, the sequence of lamellae suggested a packing model of pure components similar to the one found earlier for the *n*-$C_{30}H_{62}$/*n*-$C_{36}H_{74}$ binaries. The packing model also agreed well with the observed intensity data, given the suggested separation of the observed diffraction component from the overlapped patterns.

Introduction

The binary phase behavior of *n*-paraffins has been an important paradigm for the understanding of comiscibility of polydisperse combinations of alkane-chain-containing compounds. Binary combinations of homologous molecules, from stable solid solutions to fully phase-separated eutectics, have been shown to form a continuum of crystal structures,[1] and with no justification for the "mechanical mixture" concept once proposed for phase-separated organic crystals.[2] The molecular packing in binary arrays, in general, adapts the energetically most efficient association of component species, even when they are greatly dissimilar.

Although the characterization of *n*-paraffin binary solids by diffraction techniques has a long history (e.g., a review[3] of an already extensive literature published in 1960), it is only recently that quantitative crystal structures have been determined for various packing arrays evidenced as the volume difference between components increases. After a qualitative view of the solid solution structure was proposed from single-crystal X-ray data,[4] a representative binary solid solution structure was solved quantitatively in projection from electron diffraction intensity data.[5] More recently, a complete three-dimensional X-ray structure has been reported.[6] Multicomponent paraffin solid solutions were also shown retain the structural features of the binary solids, e.g., the quantitative electron crystallographic analyses of two petroleum waxes, a synthetic wax, and a natural mineral wax.[7]

When the volume difference between components becomes just large enough to induce instability (i.e., residing within a binodal phase boundary at ambient temperature[8]), an initially metastable solid solution can fractionate into a superlattice-like structure over days, weeks, or months.[9,10] The boundary between stable and metastable binary compositions, defined by minimum and maximum chain lengths, is very sharp.[1] Initially, the binary solid will appear to be identical to the stable paraffin solid solutions, but upon standing, the structure will gradually change as additional reflections appear in the electron diffraction pattern. The crystal structure of the final binary solid has been reported,[11] again based on electron diffraction measurements, yielding a packing model fully accordant with vibrational spectroscopic observations of lateral phase separation,[12] in addition to the more obvious longitudinal sequestering of pure components.[9] Other accounts of the longitudinal separation also have been given, based on other scattering experiments.[13] When the number of components is increased, the fractionated solid can become more complicated so that the sequence of lamellae in the superlattice is actually an array of solid solutions rather than single components.[14]

The next level of complexity is when the molecular volume difference promotes the formation of eutectic solids.[1,9] The boundary where this more rapid separation occurs, compared to the more sluggish one described in the previous paragraph, again is very sharp and can be induced just by isotopic substitution of the shorter chain length component.[8,12,15] It is known,[9] furthermore, that at least one component of the initially observed eutectic solid is a superlattice with superficial resemblance to the structure observed within the binodal phase boundary. Its crystal structure will be described in this article.

Materials and Methods

Paraffin Crystallization. Physical properties, purities, and commercial sources of the two *n*-paraffins investigated in this study, viz., *n*-triacontane (*n*-$C_{30}H_{62}$) and *n*-tetracontane (*n*-$C_{40}H_{82}$), have been reported in a previous paper.[1] The binary phase diagram has been determined[1] from a finely sampled concentration range between the two components, and X-ray and electron diffraction measurements of the lamellar spacings were plotted as a function of concentration.[1,9] In general, depending on the concentration, either one or the other pure

[⊗] Abstract published in *Advance ACS Abstracts,* June 1, 1997.

S1089-5647(96)02640-5 CCC: $14.00

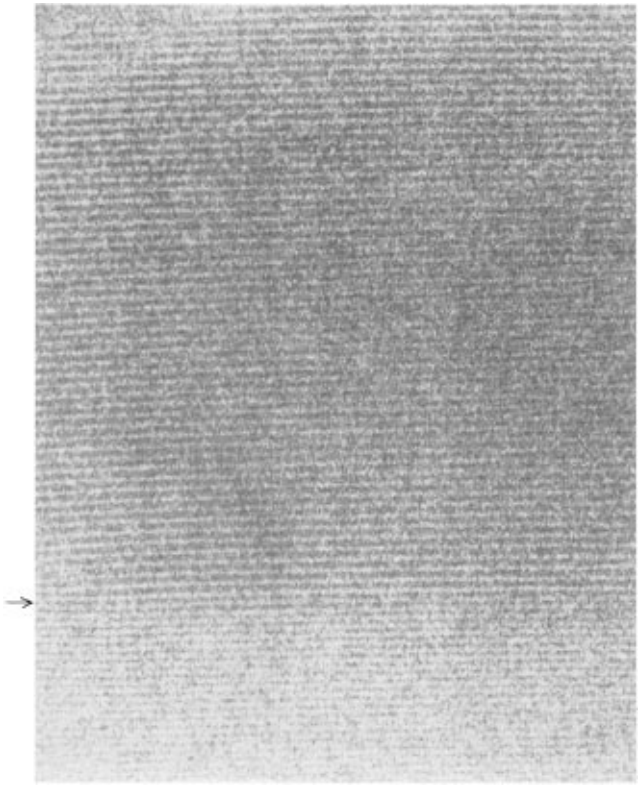

Figure 1. High-resolution electron micrograph of a nearly 1:1 *n*-$C_{30}H_{62}$/*n*-$C_{40}H_{82}$ solid (obtained by Dr. W. P. Zhang) showing lamellar stacking. The sample had been grown by epitaxial orientation. The boundary between the pure *n*-$C_{40}H_{82}$ component and a superlattice is very sharp (see arrow)—undoubtedly a tight methyl end plane interaction. However, near this boundary, laterally separated rows with narrow and wide lamellar segments can also be seen.

component separates with a superlattice structure that has an invariant average spacing over the whole concentration range.

A concentration very near a 1:1 molar combination was used for the structure determination. After making up a dilute solution of the solid in light petroleum and evaporating it on a freshly cleaved muscovite sheet, carbon-film-covered electron microscope grids were placed face down over the recrystallized solid film, and benzoic acid crystals were spread over the surface. The other half of the mica sheet was then placed over this physical mixture to make a sandwich. The sandwich was then placed on a thermal gradient, first to comelt the *n*-paraffin mixture in the benzoic acid diluent, and then rapidly cooled to cause the sequence of crystallization events that accompanies the formation of this eutectic solid.[16] The sandwich was then opened, and the benzoic acid was removed from the grids by sublimation under high vacuum. The oriented paraffin crystals could then be examined under the electron microscope. This epitaxial orientation procedure is an adaptation of the method given by Wittmann, Hodge, and Lotz.[17]

Electron Crystallographic Determination. Procedures for electron crystallographic analysis have been reviewed in a recent monograph.[18] Selected area electron diffraction patterns were obtained from the oriented paraffin films at 100 kV with a JEOL JEM-100CXII electron microscope and recorded on Kodak DEF-5 X-ray film. (In previous work, low-dose electron micrographs of the binary paraffin microcrystals had also been obtained by Dr. W. P. Zhang using samples that had been deposited onto a crystalline substrate from the vapor phase.[19] Procedures for recording such "lattice images" of radiation-sensitive aliphatic molecular crystals have been reviewed recently.[18] A representative image is shown in Figure 1.) Electron diffraction intensities were obtained by integration of scans of the diffraction films by a Joyce-Loebl Mk.IIIC flat-bed microdensitometer. No Lorentz correction was required.[18] Diffraction spacings were calibrated against a gold powder standard.

Crystal structures of *n*-paraffins have been obtained from electron diffraction intensities by direct phasing methods.[20] In this particular problem, the initial task was to separate a composite diffraction pattern into its components. That of the pure paraffin *n*-$C_{40}H_{82}$ could be isolated in some cases, but the superlattice contribution, when observed clearly, was always included with the pattern from the pure longer component. In principle, the most intense reflections of the 0*kl* pattern, shared by both *n*-$C_{40}H_{82}$ and superlattice, could be deconvoluted, if the weights m_i of $m_1I_1 + m_2I_2$ for the diffraction intensities of the overlapped components were known.[21] However, these weights cannot be determined simply. Instead, the strong 0*kl* "polyethylene" reflections from *n*-$C_{40}H_{82}$ were reindexed to the superlattice repeat (see below). Since the first lamellar reflection intensity of *n*-$C_{40}H_{82}$ or the superlattice was observed to be nearly equal, the strong reflections were added to the separable superlattice 00*l* row with the same weight as found for the separable longer paraffin component. This reconstructed data set was used for structure analysis.

The crystal structure of the pure paraffin was solved, knowing the structure expected for a shorter homolog.[22] After segregation of the 00*l* signal for the superlattice, a unit cell length was found that would give a nearly integral index to the lamellar reflections. Crystallographic phases were given to these 00*l* reflections, according to the envelope found in the analysis of a pure paraffin structure,[20] and these phased reflections were used to calculate the reverse Fourier transform, showing the repetitive array of lamellar longitudinal cross sections within the long repeat. A paraffin chain packing model was then constructed, based on the maxima and minima of these lamellar features, using also the known lamellar spacings of pure paraffins in orthorhombic crystal structures.[23] This model was then used to calculate structure factors for the entire 0*kl* pattern.

Results

Earliest low-dose electron microscopic studies[9] of this binary solid revealed that the superlattice and longer chain pure component could exist as tightly associated domains that were oriented in the same way. As shown in Figure 1, a higher-resolution image[19] revealed that the boundary between these two crystalline regions should be quite intimate, probably involving an exact epitaxial match across identical methyl end planes at the lamellar interface.

Electron diffraction patterns from the pure *n*-$C_{40}H_{82}$ domains were found to be characteristic of the orthorhombic even chain paraffins (Figure 2a). The intense 01*l* reflections could be indexed according to an $l = m$, $m + 2$ rule,[24] where m is the carbon number *n*-C_mH_{2m+2} of each lamellar layer (i.e., $m = 40$, in this example). Lamellar spacings measured from a number of representative diffraction patterns gave $c/2 = 52.49 \pm 0.14$ Å, in good agreement with the literature value (52.65 Å) for this paraffin.[23] (N.b.: 1.0 Å = 0.1 nm.) From the observed systematic absences, it was clear that the space group must be $Pca2_1$.

The crystal structure was solved after construction of an ideal chain packing, using procedures given by Nyburg and Potworowski[23] and adapted from the orthorhombic crystal structure of the *n*-$C_{36}H_{74}$ homolog.[22] The unit cell constants were $a = 7.42$, $b = 4.96$, and $c = 104.98$ Å. When isotropic temperature factors were assigned to the two types of atoms, $B_C = 6.0$ Å^2 and $B_H = 8.0$ Å^2, the crystallographic residual was calculated

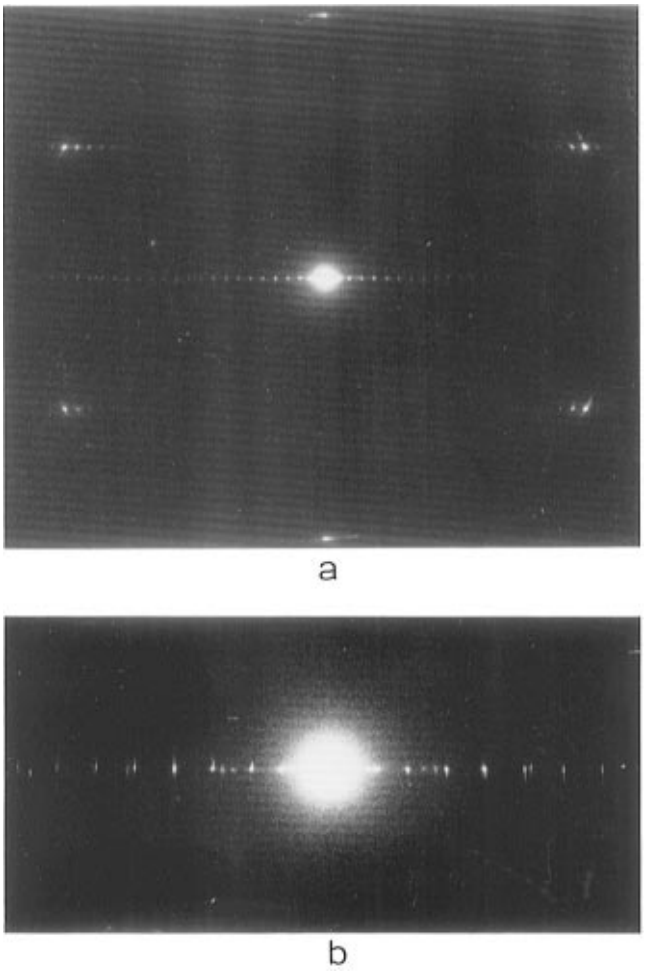

Figure 2. Electron diffraction patterns from epitaxially oriented n-$C_{30}H_{62}$/n-$C_{40}H_{82}$ solids: (a) Isolated n-$C_{40}H_{82}$ component—complete 0kl pattern; 00l lamellar reflections have a single repeat spacing. (b) In the patterns from n-$C_{30}H_{62}$/n-$C_{40}H_{82}$ superlattice + longer chain component, the complete 0kl pattern superficially resembles that of pure n-$C_{40}H_{82}$. However, the lamellar row of the mixed component pattern also contains superlattice reflections.

TABLE 1: Observed and Calculated Structure Factors for the n-$C_{40}H_{82}$ Component of the Eutectic Solid

0kl	$\|F_o\|$	$\|F_c\|$	0kl	$\|F_o\|$	$\|F_c\|$
00 2	0.64	0.34	00 38	0.23	0.09
00 4	0.59	0.32	00 80	0.47	0.24
00 6	0.53	0.32	00 82	1.12	1.12
00 8	0.64	0.33	00 84	0.90	0.41
00 10	0.57	0.36	01 34	0.26	0.26
00 12	0.44	0.38	01 36	0.28	0.34
0014	0.42	0.36	01 38	0.43	0.52
00 16	0.47	0.30	01 40	0.87	1.21
00 18	0.43	0.27	01 42	1.38	1.94
00 20	0.30	0.20	01 44	0.37	0.44
00 22	0.33	0.20	02 0	2.92	3.05
00 24	0.33	0.25	02 2	0.31	0.06
00 26	0.29	0.28	02 4	0.22	0.09
00 28	0.31	0.29	02 82	0.76	0.37
00 30	0.30	0.29	02 84	0.65	0.15
00 32	0.23	0.23	03 40	0.55	0.56
00 34	0.18	0.15	03 42	0.94	0.94
00 36	0.22	0.08			

to be $R = 0.28$. A comparison of calculated and observed data is given in Table 1. The crystal structure, projected along [100] is shown in Figure 4.

Diffraction patterns containing a contribution from the superlattice component were more complicated in appearance (Figure 2b), but the lamellar row had an unmistakable overlay

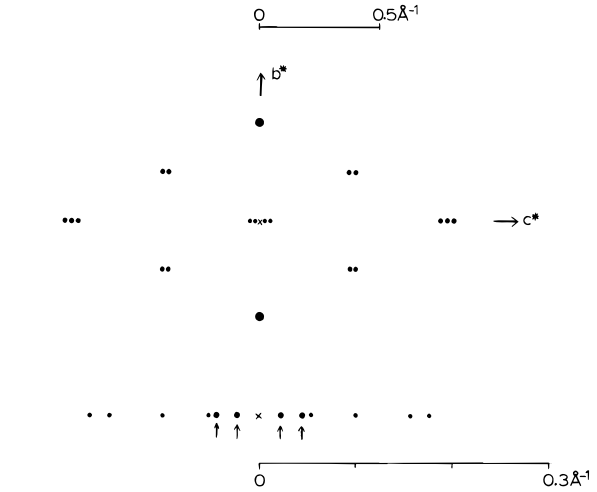

Figure 3. Schematic representation of superlattice pattern, separated from composite 0kl pattern in Figure 2b. Top: overview with two inner-order 00l lamellar repeats at (004) and (008) without superlattice components. Bottom: magnification of the 00l row with additional superlattice reflections that are not a regular repeat of (00,4n); see Table 2. The (004) and (008) reflections of the above figure are indicated by arrows. Scales of the two patterns are shown at the top and bottom, respectively.

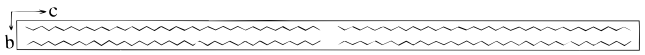

Figure 4. Crystal structure of n-$C_{40}H_{82}$ in a projection down [100].

TABLE 2: Lamellar Superlattice Phases for C_{30}/C_{40} Domain of Eutectic; (1) c = 174.68 Å and (2) c = 172.50 Å

l(1)	d^*_{obs}	d^*_{calc}(1)	l(2)	d^*_{calc}(2)	$\|F_{obs}\|$	phase
4	0.0229	0.0229	4	0.0232	0.66	π
8	0.0461	0.0458	8	0.0464	0.32	π
9	0.0528	0.0515	9	0.0522	0.47	π
17	0.0994	0.0973	17	0.0986	0.39	π
26	0.1515	0.1488	26	0.1507	0.32	π
31	0.1757	0.1775	30	0.1739	0.26	π
131[a]	0.7620	0.7499	130	0.7536	0.47	0
135[a]	0.7811	0.7728	134	0.7768	1.12	0
138[a]	0.8002	0.7900	138	0.8000	0.90	π

[a] Also components of n-$C_{40}H_{82}$ pattern.

of contributions from both the pure and mixed chain domains. For structure analysis the regular repeat due to n-$C_{40}H_{82}$ was removed from the lamellar row. The remaining superlattice pattern (including the conserved polymethylene scattering component) is drawn schematically in Figure 3. After finding approximate Miller indices (initially assuming c = 174.68 Å, see Table 2), the remaining 00l amplitudes were then assigned crystallographic phases, assuming that they matched the values for n-$C_{40}H_{82}$ as a continuous envelope. It was assumed, therefore, that the superlattice was nearly commensurate. After calculating the reverse transform, the lamellar array in Figure 5 was observed. A model based on sequestered n-$C_{30}H_{62}$ and n-$C_{40}H_{82}$ layers was suggested (Figure 5), resembling closely the earlier determined n-$C_{30}H_{62}$/n-$C_{36}H_{74}$ superlattice.[11] A packing model of paraffin chains was then constructed, again using the geometrical constraints in Figure 4 for individual lamellae and their longitudinal sequence. For construction of a chain packing model that fit within the block structure of Figure 6 (delineating domains of pure n-$C_{30}H_{62}$ and n-$C_{40}H_{82}$ components), the unit cell constants of the lateral chain packing were the same as those of the pure $C_{40}H_{82}$ component, but the symmetry operations applied to the individual chain layers were x, y, z; $^1/_2 + x, -y, z$. The lamellar interfaces were constructed to conform to the geometrical requirements of the even-chain

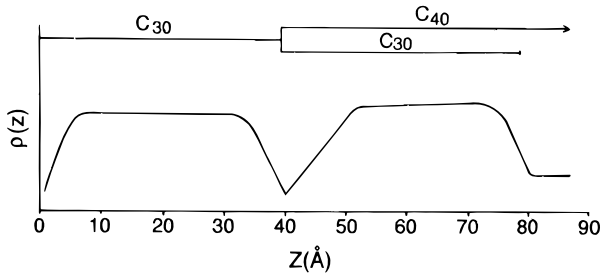

Figure 5. One-dimensional Fourier transform of initial lamellar index estimate (assuming $c = 174.68$ Å; see Table 2). A lamellar sequence of n-$C_{30}H_{62}$ and n-$C_{40}H_{82}$ components is drawn for half of the unit cell repeat. Note the deep and shallow "troughs" of density between lamellar projections. The interpretation follows a similar analysis in ref 11.

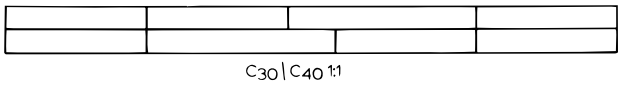

Figure 6. Superlattice model for 1:1 n-$C_{30}H_{62}$/n-$C_{40}H_{82}$ expressed as blocks of pure components. The lateral phase separation is depicted in the central region of this unit cell representation. Blocks are drawn at the lengths of the pure paraffin components.

TABLE 3: Calculated and Observed Structure Factors from Superlattice Model

00*l*	$\|F_o\|$	$\|F_c\|$	00*l*	$\|F_o\|$	$\|F_c\|$
00 4	0.66	0.30	00 138	0.90	0.83
00 8	0.32	0.16	01 65	0.87	0.57
00 9	0.47	0.30	01 69	1.38	1.33
00 17	0.39	0.29	02 0	2.92	3.05
00 26	0.32	0.34	02 134	0.76	0.55
00 30	0.26	0.28	02 138	0.65	0.44
00 130	0.47	0.22	03 65	0.55	0.61
00 134	1.12	1.06	03 69	0.94	1.41

orthorhombic paraffins. (See also specifications given in ref 11.) Note that there again must be a lateral segregation of the long and short components in some layers, as found in the superlattice structure determined earlier.[11] At this point a slight readjustment was made in the lamellar spacing to $c = 172.50$ Å (see Table 2 for the effect on the indices and calculated d^* values) because it gave an improved agreement to the observed lamellar spacings.

For the calculation of structure factors, as stated above, the strong 0*kl* reflections of the pure component were used as a first approximation of the nonlamellar intensity from the pure superlattice domain. (Again, this was never observed as a separate entity in this study.) The form and scaling of this reconstructed 0*kl* pattern was also justified from the previous quantitative study[11] of n-$C_{30}H_{62}$/n-$C_{36}H_{74}$, as well as a number of pure orthorhombic (even or odd) paraffins and their solid solutions.[5,7,20] (This is the most "conservative" part of the diffraction pattern since the strongest 0*kl* reflections originate from the "polyethylene" repeat of the methylene subcell.) With this approximation assumed to be nearly correct, the match of this packing model to the observed data was actually quite good (Table 3), where $R = 0.21$, based on the positions of carbon chain skeletons, where $B_C = 2.0$ Å^2.

Discussion

From accumulated studies of paraffin binary solids, it has been shown that the sequence of structures from fully cosoluble to fully fractionated components involves a continuously subtle variation of packing schemes, yet preserving features of arrays for neighboring binary solids found across the instability boundaries. At the first onset of fractionation, when a solid freshly crystallized from the melt is held within a binodal phase boundary, there is a sluggish rearrangement, perhaps by longitudinal diffusion, to the superlattice with a sequencing of pure chain layers (but also with some resultant lateral phase separation). This array is complicated by the presence of more than two components, so that the initial segregation is a layering of solid solutions.[14]

As shown in this atomic-resolution study of the initial eutectic solid formed as the volume difference between chain components is gradually increased, either the longer or shorter pure component exists at a tight epitaxial boundary, i.e., a matching of methyl end planes at the lamellar interface, with a superlattice that is now known to be very similar to the one formed from the metastable solid solutions.[11] Again, some layers must pack with islands of pure paraffin embedded in domains of the other component, even though the separation rate of the components is much faster in this case. The growth of lateral domains implied by the model is in line with earlier vibrational spectroscopic measurements on $C_{30}D,H/C_{36}D,H$ binaries where isotopic substitution (meaning H for perprotonated and D for perdeuterated) is used as a variable.[25] When both components are hydrogenated or deuterated or when the longer component is deuterated, the phase separation is virtually the same as described for all other metastable solid solutions.[1] However, perdeuteration of the shorter component creates a binary that behaves more like $C_{30}H_{62}/C_{40}H_{82}$ (also seen by comparison of the phase diagrams[1,15]) in that it forms a eutectic solid. Nevertheless, the phase separation still contains a marked lateral component in addition to the longitudinal sequencing of lamellae observed in the earliest diffraction studies of such solids. Evidence for such lateral separation is also found from reinspection of the micrograph in Figure 1. For example, near the boundary between superlattice and pure n-$C_{40}H_{82}$ (see arrow), narrow and wide lamellar segments can be seen in a single row.

Because the number of atoms used to construct the superlattice model is rather large (140 in carbons in the asymmetric unit), it might be thought that the close fit to the experimental data may be due to an overparametrization[26] of the model, since the number of observed diffraction maxima is far less than the atomic positions. However, the model was treated as a theoretical chain "diffraction grating", placing atoms only at ideal positions. The unique chains themselves, as rigid bodies, are in fact the experimental variables, incorporating only a group isotropic temperature factor. There is no ambiguity for the chain positions within a layer but only in how the adjacent layers in a laterally separated lamella will pack next to one another. Obviously, there must be a continuous, flat methyl end plane on any mixed lamellar surface—a feature that imposes yet another constraint on modeling. The sequencing of lamellae is only an average positioning suggested by the block structure in Figure 6. However, there may local variations of this sequence in the real structure that cannot be detected from a crystal structure analysis. Hence, the model is more conceptual than a detailed representation of possible local variations.

As the volume difference of the chains increases further, i.e., when no cosolubility is possible, only the two pure components will cocrystallize. Even in this case, there is already evidence for a tight epitaxial boundary between the crystalline domains.[27] Thus, the formation of these structures continuously attempts to minimize nonoverlap volume of the components, starting from stable solid solutions to fully fractionated eutectic solids.

Acknowledgment. Research was supported by a grant from the National Science Foundation (CHE94-17835) which is gratefully acknowledged. Dr. W. P. Zhang is thanked for originally obtaining the electron micrograph in Figure 1.

References and Notes

(1) Dorset, D. L. *Macromolecules* **1990**, *23*, 623.
(2) Hsu, E. C. H.; Johnson, J. F. *Mol. Cryst. Liq. Cryst*. **1974**, *27*, 95.
(3) Mnyukh, Yu. V. *Zh. Strukt. Khim*. **1960**, *1*, 370.
(4) Lüth, H.; Nyburg, S. C.; Robinson, P. M.; Scott, H. L. *Mol. Cryst. Liq. Cryst*. **1974**, *27*, 337.
(5) Dorset, D. L. *Proc. Natl. Acad. Sci. U.S.A.* **1990**, *87*, 8541.
(6) Gerson, A. R.; Nyburg, S. C. *Acta Crystallogr*. **1994**, *B50*, 252.
(7) Dorset, D. L. *Acta Crystallogr*. **1995**, *B51*, 1021. Dorset, D. L. *J. Phys. D, Appl. Phys*. **1997**, *30*, 451.
(8) Snyder, R. G.; Conti, G.; Strauss, H. L.; Dorset, D. L. *J. Phys. Chem*. **1993**, *97*, 7342.
(9) Dorset, D. L. *Macromolecules* **1986**, *19*, 2965.
(10) Mazee, W. M. *Am. Chem. Soc. Div. Petrol. Chem. Prepr*. **1958**, *3* (4), 35.
(11) Dorset, D. L.; Snyder, R. G. *J. Phys. Chem*. **1996**, *100*, 9848.
(12) Snyder, R. G.; Goh, M. C.; Srivatsavoy, V. J. P.; Strauss, H. L.; Dorset, D. L. *J. Phys. Chem*. **1992**, *96*, 10008.
(13) Annis, B. K.; Londono, J. D.; Wignall, G. D.; Snyder, R. G. *J. Phys. Chem*. **1996**, *100*, 1725.
(14) Dorset, D. L.; Conti, G.; Snyder, R. G. Manuscript in preparation.
(15) Dorset, D. L.; Snyder, R. G. *Macromolecules* **1995**, *28*, 8412.
(16) Dorset, D. L.; Hanlon, J.; Karet, G. *Macromolecules* **1989**, *22*, 2169.
(17) Wittmann, J. C.; Hodge, A. M.; Lotz, B. *J. Polym. Sci., Polym. Phys. Ed*. **1983**, *21*, 2495.
(18) Dorset, D. L. *Structural Electron Crystallography*; Plenum: New York, 1995.
(19) Zhang, W. P.; Dorset, D. L. *Proceedings of the 47th Annual Meeting of the Electron Microscopy Society of America*; San Francisco Press: San Francisco, 1989; pp 702−703.
(20) Dorset, D. L.; Zemlin, F. *Ultramicroscopy* **1990**, *33*, 227. Dorset, D. L.; Zhang, W. P. *J. Electron Microsc. Technol*. **1991**, *18*, 142.
(21) Tadokoro, H. *Structure of Crystalline Polymers*; Wiley-Interscience: New York, 1979; p 59.
(22) Teare, P. W. *Acta Crystallogr*. **1959**, *12*, 294.
(23) Nyburg, S. C.; Potworowski, J. A. *Acta Crystallogr*. **1973**, *B29*, 347.
(24) Dorset, D. L. *Macromolecules* **1987**, *20*, 2782.
(25) Snyder, R. G.; Srivatsavoy, V. J. P.; Cates, D. A.; Strauss, H. L.; White, J. W.; Dorset, D. L. *J. Phys. Chem*. **1994**, *98*, 674.
(26) Hamilton, W. C. *Statistics in Physical Science*; Ronald: New York, 1964; pp 157−160.
(27) Dorset, D. L. *J. Polym. Sci. B: Polym. Phys*. **1989**, *27*, 1161.